colloids and interfaces

MDPI

Article

Bio-Pesticidal Potential of Nanostructured Lipid Carriers Loaded with Thyme and Rosemary Essential Oils against Common Ornamental Flower Pests

Alejandro Múnera-Echeverri [1,*], José Luis Múnera-Echeverri [2] and Freimar Segura-Sánchez [1,*]

[1] Biopolimer Research Group, Department of pharmacy, Faculty of Pharmaceutical and Food Sciences, University of Antioquia, Calle 70 No. 52–21, Medellín 050001, Colombia
[2] Ecofresca Flowers SAS, Avenida Carvajal No. 31–12, San Vicente Ferrer 054010, Colombia; jose.luis.munech@gmail.com
* Correspondence: alejandro.munerae@udea.edu.co (A.M.-E.); freimar.segura@udea.edu.co (F.S.-S.)

Abstract: The encapsulation of essential oils (EOs) in nanostructured lipid carriers (NLCs) represents a modern and sustainable approach within the agrochemical industry. This research evaluated the colloidal properties and insecticidal activity of NLCs loaded with thyme essential oil (TEO-NLC) and rosemary essential oil (REO-NLC) against three common arthropod pests of ornamental flowers: *Frankliniella occidentalis*, *Myzus persicae*, and *Tetranychus urticae*. Gas chromatography–mass spectrometry (GC-MS) analysis identified the major chemical constituents of the EOs, with TEO exhibiting a thymol chemotype and REO exhibiting an α-pinene chemotype. NLCs were prepared using various homogenization techniques, with high shear homogenization (HSH) providing the optimal particle size, size distribution, and surface electrical charge. A factorial design was employed to evaluate the effects of EO concentration, surfactant concentration, and liquid lipid/solid lipid ratio on the physicochemical properties of the nanosuspensions. The final TEO-NLC formulation had a particle size of 347.8 nm, a polydispersity index of 0.182, a zeta potential of −33.8 mV, an encapsulation efficiency of 71.9%, and a loading capacity of 1.18%. The REO-NLC formulation had a particle size of 288.1 nm, a polydispersity index of 0.188, a zeta potential of −34 mV, an encapsulation efficiency of 80.6%, and a loading capacity of 1.40%. Evaluation of contact toxicity on leaf disks showed that TEO-NLC exhibited moderate insecticidal activity against the western flower thrips and mild acaricidal activity against the two-spotted spider mite, while REO-NLC demonstrated limited effects. These findings indicate that TEO-NLCs show potential as biopesticides for controlling specific pests of ornamental flowers, and further optimization of the administration dosage could significantly enhance their effectiveness.

Keywords: nanostructured lipid carrier; essential oils; high shear homogenization; biopesticide

Citation: Múnera-Echeverri, A.; Múnera-Echeverri, J.L.; Segura-Sánchez, F. Bio-Pesticidal Potential of Nanostructured Lipid Carriers Loaded with Thyme and Rosemary Essential Oils against Common Ornamental Flower Pests. *Colloids Interfaces* **2024**, *8*, 55. https://doi.org/10.3390/colloids8050055

Academic Editors: Aleksandra Szcześ, Wuge Briscoe, Reinhard Miller and Milad Radiom

Received: 19 August 2024
Revised: 26 September 2024
Accepted: 8 October 2024
Published: 12 October 2024

1. Introduction

Nanotechnology has revolutionized many industries, including pharmaceuticals, foods, cosmetics, and agrochemicals [1–4]. In the pharmaceutical industry, nanoparticles technology is essential for drug delivery to target tissues and other functional roles. Among those nanoparticles, solid lipid nanoparticles (SLNs) and nanostructured lipid carriers (NLCs) provide a stable delivery system for active ingredients and improve their bioavailability [5,6]. Essential oils (EOs) are special active ingredients valued for their biological properties. These oils have gained significant interest in various fields, including pharmaceuticals and cosmetics, due to their natural and safe status, broad acceptance by consumers, and versatile functional properties [7]. In recent years, there has been a growing interest in the use of EOs as biopesticides for pest control [8]. These compounds have demonstrated important bio-pesticidal properties, such as insecticidal, fungicidal, and antimicrobial effects [9]. Furthermore, EOs are biodegradable and pose less risk to the

environment and human health compared to synthetic chemical pesticides. The use of EOs for pest control can provide a promising solution to address the challenges of pesticide resistance, environmental pollution, and human health concerns [10]. However, their volatility and sensitivity to light, heat, and oxidation present challenges for their application. To address these challenges, encapsulating EOs in SLNs and NLCs has emerged as a promising approach to overcome these limitations [11] and represents a modern and sustainable alternative to synthetic chemical pesticides within the agrochemical industry [12].

Agrochemicals consumption is particularly high in the ornamental flower industry to meet aesthetic and production demands, reflecting its intensive production practices [13]. The global floriculture industry, encompassing cut flowers, potted flowering plants, and propagation materials like seeds and bulbs, is a thriving market with a dynamic growth trajectory and substantial financial returns, exceeding an estimated USD 100 billion in annual trade value [14]. Colombia is well-known for its diverse ornamental flower industry, which significantly contributes to the country's agricultural economy. As one of the world's leading producers and exporters of cut flowers, Colombia's ornamental flower sector encounters distinct challenges, especially the management of pests that can threaten the quality and exportability of the flowers [15]. A study conducted in the Antioquia region found that a significant number of hydrangea flower samples contained limiting pests, which posed a risk to the industry's access to international markets. The study identified mites, along with their eggs and mobile stages, as the most prevalent arthropod pests. However, the prevalence of aphids, thrips, and slugs was also significant [16].

The aim of this work was to develop EO-NLC formulations as potential biopesticides against three key arthropod pests of ornamental flowers: *Frankliniella occidentalis* (Western flower thrips), *Myzus persicae* (green peach aphid), and *Tetranychus urticae* (two-spotted spider mite). The study involved the extraction by steam distillation of *Thymus vulgaris* EO (TEO) and *Rosmarinus officinalis* EO (REO) and the preparation of NLC dispersions through various methods, including high shear homogenization (HSH), ultrasound homogenization (USH), and hot high-pressure homogenization (HHPH). We utilized a 2^3 factorial design to study the influence of the EO concentration, surfactant concentration, and the liquid lipid/solid lipid ratio on some colloidal properties. The formulations were analyzed for particle size, polydispersity index, zeta potential, encapsulation efficiency, loading capacity, and thermal properties to achieve optimal physicochemical characteristics. These formulations were evaluated for their contact toxicity effects against the arthropod pests.

2. Materials and Methods

2.1. Materials

Thyme (*Thymus vulgaris*) and rosemary (*Rosmarinus officinalis*) plants were harvested from a commercial plantation located in Rionegro, Antioquia, Colombia (6°12′00.6″ N 75°21′33.5″ W). The mean annual temperature of the municipality is 18 °C, the mean annual precipitation is 2100 mm, and the dominant soil is derived from volcanic ash.

Carnauba wax (CW) and thymol were purchased from Sigma-Aldrich, St. Louis, MO, USA. Miglyol (MIG) was provided by Cremer oleo GmbH & Co., Hamburg, Germany. Tween 80 (T80), 1,8-cineol, chloroform, dichloromethane, acetone and ethanol were purchased from Merck, Boston, MA, USA.

2.2. Essential Oil Extraction

Thyme and rosemary freshly harvested plant material was ground using an agro-industrial chopper and then extracted by steam distillation using semi-industrial distillation equipment. The extractor vessel was filled with a packed fixed bed made of crushed fresh plant leaves and stems. Slightly superheated steam at approximately 102 °C was generated in a propane gas-fired boiler. Once the desired temperature was reached, a valve was opened to inject the steam through a distributor at the bottom of the vessel. This process heats the raw material, causing the volatile components of the plant to vaporize. The entire distillation process took approximately 3 h. Afterward, TEO and REO were separated

from the aqueous phase, dehydrated with anhydrous sodium sulfate, preserved in airtight containers, protected from light exposure, and stored at 4 °C. A scheme of the extraction process is shown in Figure 1.

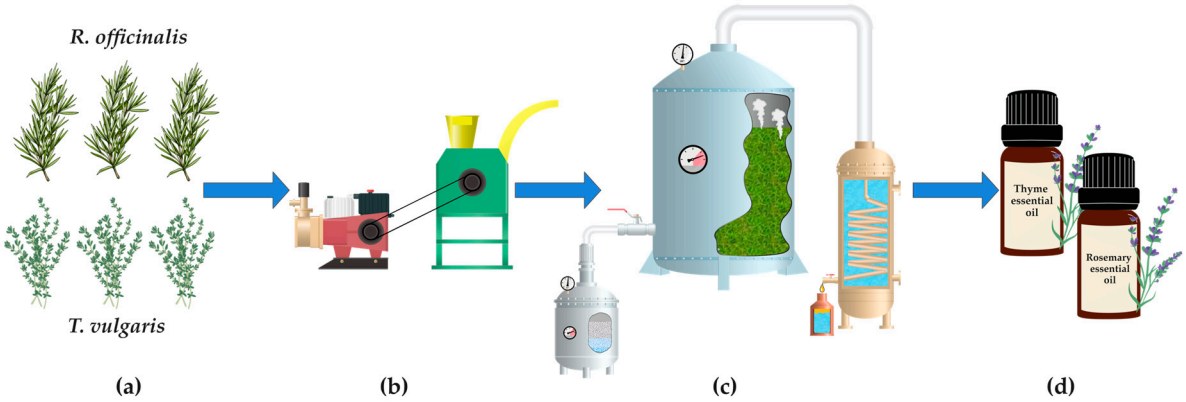

Figure 1. Scheme of extraction process to obtain TEO and REO: (**a**) thyme and rosemary freshly harvested plant material; (**b**) grinding step by agro-industrial chopper; (**c**) distillation equipment: boiler–extractor vessel–condenser–collector; (**d**) thyme EO and rosemary EO.

2.3. Characterization of Essential Oil's Chemical Composition

The chemical characterization of the EOs was carried out using gas chromatography coupled to mass spectrometry (GC-MS). Samples were prepared via dilution with dichloromethane. A certified C6–C25 hydrocarbon mixture (AccuStandard, New Haven, CT, USA) was used as the reference material. Chromatographic analysis was performed using an Agilent Technologies 6890 gas chromatograph coupled with a mass selective detector (MSD, AT 5973N) (Agilent Technologies, Inc., Santa Clara, CA, USA), operated in full scan mode. Injection was performed in split mode (30:1), injection volume, V_{inj} = 2 µL. The column used in the analysis was a DB-5MS (J & W Scientific, Folsom, CA, USA), 5%-Ph-PDMS, 60 m × 0.25 mm × 0.25 µm. The presumptive identification of the compounds detected in the samples was based on their mass spectra (EI, 70 eV) and fragmentation patterns, using the Adams, Wiley, and NIST databases.

2.4. Preparation of NLC Dispersions

Initially, three methods of colloidal system production were tested: HSH, USH, and HHPH. All methods shared the HSH stage and were tested with a previously developed formulation consisting of 20% organic phase, 4% surfactant, and 2% EO. The NLCs were prepared using procedures adapted from Khezri, Souto, and Baldim studies [17–19],which involved HSH, USH, and HHPH with some modifications.

First, the surfactant and water were weighed into a glass container as the aqueous phase, while the wax, liquid lipid, and EOs were weighed separately in different containers. The wax was heated until melted at 82 °C, and the aqueous phase was heated to a temperature 5–10 °C higher than the melting point of the wax. After warming for one minute, the liquid lipid and EO blend was mixed with the melted wax before adding the aqueous phase. HSH was carried out using an Ultraturrax T25 mixer (IKA, Staufen im Breisgau, Germany) starting at 2800 rpm speed and gradually increasing to 25,000 rpm for five minutes. Following this step, the resulting hot colloidal emulsion was allowed to cool down to room temperature (RT). In USH, the hot pre-emulsion was sonicated using a Branson 250 ultrasonic probe (Branson Ultrasonics Corp., Brookfield, CT, USA) at 90% amplitude for one minute; then, the resulting colloidal emulsion was cooled to RT. In HHPH, the hot pre-emulsion was passed once through a pre-heated Emulsiflex C3 homogenizer (Avestin Inc., Ottawa, Canada) at 1500 bar; then, the resulting colloidal emulsion was cooled to RT.

Free EO NLCs (FEO-NLC) dispersions were prepared using the same procedure as described above. FEO-NLC formulation was produced to evaluate the thermal behavior of

systems without essential oils and to serve as a control in toxicity tests against arthropods. A scheme of the preparation process is shown in Figure 2.

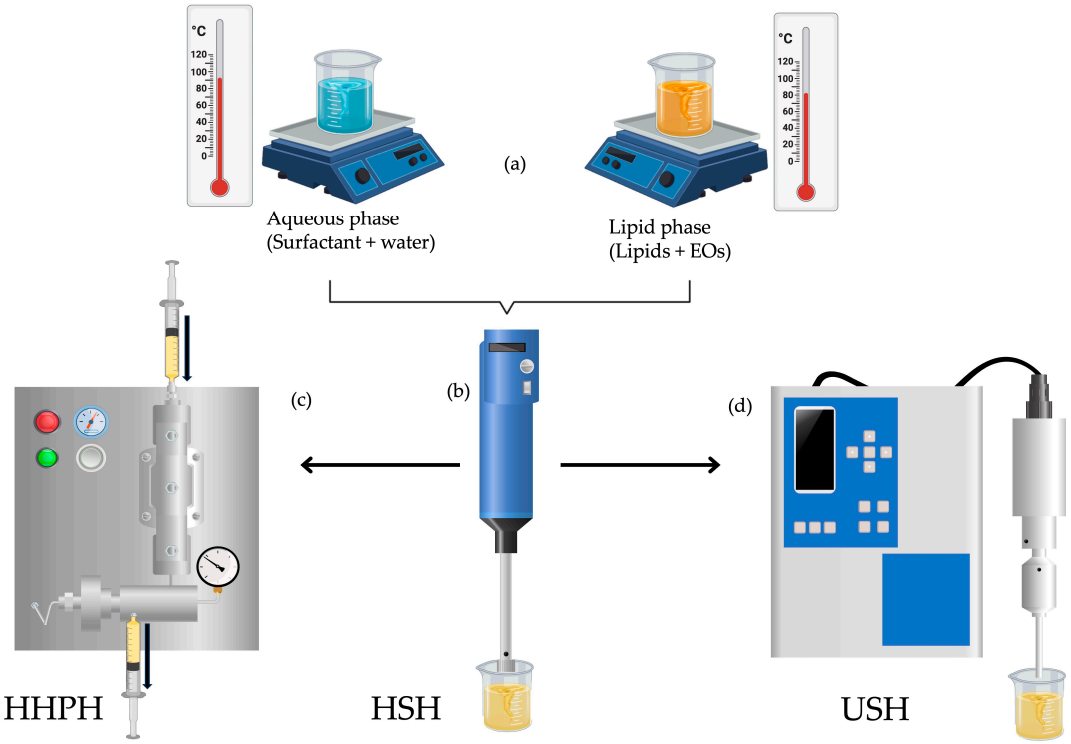

Figure 2. Experimental scheme of NLCs production: (**a**) heating aqueous phase and organic phase separately; (**b**) mixing and homogenization of both phases by HSH; (**c**) homogenization of hot pre-emulsion by HHPH; (**d**) homogenization of hot pre-emulsion by USH.

2.5. Factorial Design

A 2^3 factorial design with four central points was carried out to evaluate the effect of (A) the concentration of EO (%*w*/*w*); (B) the concentration of T80 (%*w*/*w*); and (C) the liquid lipid/solid lipid ratio (LL/SL) on (1) particle size; (2) PDI; and (3) Zeta potential.

Table 1 presents the factor levels as a percentage of each component in the formulations.

Table 1. Levels of the independent variables (factors).

Factors	Levels		
	−	**0**	**+**
A: Essential oil, %*w*/*w*	1	2	3
B: Tween 80, %*w*/*w*	3	4	5
C: LL/SL (Liquid lipid/Solid lipid)	15/85	20/80	25/75

The results were analyzed using ANOVA and a response surface model using R (R 4.1.3, R Core Team, 2022) Table S1 shows the composition and codification of each formulation. Table S2 indicates the MIG/EO ratio in the NLC formulations of the factorial design (See Supplementary Data).

2.6. Characterization of NLC

2.6.1. Particle Size, Polydispersity Index, and Zeta Potential Determination

Mean particle size and particle size distribution were characterized by Dynamic light scattering (DLS) and surface charge was characterized electrophoretic light scattering (ELS). The Zetasizer Nano ZS90 equipment (Malvern Instruments, Worcestershire, United Kingdom) was employed to measure the average particle size, polydispersity index, and zeta

potential. To ensure accuracy and repeatability, each sample underwent a 1:1000 dilution in Type I water before measurements. Each sample was measured three times at 25 °C.

2.6.2. Morphological and Structural Characterization

A dilution of 1:5000 of the NLCs in type I water was prepared for SEM and TEM analyses.

The morphology and surface roughness of NLCs were analyzed via scanning electron microscopy (SEM). The samples were fixed on a graphite tape, coated with gold (Au) using a DENTON VACUUM Desk IV equipment (Denton Vacuum Inc., Moorestown, NJ, USA), and analyzed using a JEOL JSM 6490 LV scanning electron microscope (Jeol Ltd., Tokyo, Japan), with an accelerating voltage of 20 kV under high vacuum to obtain high-resolution images. The secondary electron detector was employed to evaluate the morphology and topography of the samples.

The structure and morphology of NLCs were analyzed via transmission electron microscopy (TEM). A small volume of the diluted NLC suspension was placed onto a copper grid coated with a film of formvar carbon. The grid was allowed to air dry for several minutes to allow the NLCs to adhere to it. Once the grids were dry, they were immersed in a drop of uranyl acetate for 8 min and then washed several times in containers with type I water. Excess water was removed from the grid using filter paper. Subsequently, images of the NLCs were captured using a Tecnai F20 Super Twin TMP transmission electron microscope(FEI Company, Hillsboro, OR, USA) with an accelerating voltage of 80 kV.

2.6.3. Encapsulation Efficiency and Loading Capacity

The chromatographic analysis was conducted using an Agilent Technologies 7890 A gas chromatograph (Agilent Technologies, Inc., Santa Clara, CA, USA). Injection was performed in split mode (50:1), V_{inj} = 1 µL. The column used was DB-5 (Agilent Technologies, Inc., Santa Clara, CA, USA), 30 m × 0.25 mm × 0.25 µm, with an FID detector. The carrier gas was hydrogen at 1 mL/min. The oven temperature started at 40 °C for 3 min and then increased by 5 °C/min to a final temperature of 160 °C, which was held for 1 min. The detector temperature was 260 °C. A series of standard solutions with known concentrations of the marker compound (thymol and 1,8-cineole for TEO and REO, respectively) were prepared in chloroform, with the same solvent used to dissolve the NLCs. The calibration curve for each marker was established in a concentration range between 1 to 2000 ppm and performed in triplicate.

Encapsulation Efficiency

Encapsulation efficiency measures the amount EO encapsulated within the NLCs relative to the total amount of EO added to the system. Since EO is a mixture of many compounds, a marker compound was chosen to quantify and indicate the approximate amount of encapsulated EO.

A known amount of the NLC suspension was circulated through a tangential flow filtration (TFF) system with a 0.22 µm polyethersulfone (PES) membrane at a flow rate of 10 mL/min, and the filtrate was collected. This filtrate was then placed in the upper chamber of a Pierce™ 10 K MWCO protein concentrator tube (Thermo Fisher Scientific, Waltham, MA, USA). The system was centrifuged at 10,000 rpm for 15 min, after which 0.5 mL of the separated fraction collected at the bottom of the tube (filtrate) underwent liquid–liquid extraction with chloroform. The organic phase was subjected to GC to quantify the free marker compound.

Separately, 1 mL of the NLC suspension was mixed with 1 mL of chloroform in a 2 mL Eppendorf tube. The mixture was sonicated and heated to 45 °C for 10 min in a sonication bath to dissolve the nanoparticles and extract the total EO present in the formulation through liquid–liquid extraction. Subsequently, centrifugation at 14,000 rpm for 30 min at 4 °C was performed to separate the wax from the chloroform, and the organic phase

was removed from the Eppendorf tube. The organic phase was subjected to GC to quantify the total amount of the marker compound in the formulation. Equation (1) was used to calculate the encapsulation efficiency.

$$\%EE = \frac{[(Total\ marker\ compound\ in\ the\ formulation) - (free\ marker\ compound)]}{(marker\ compound\ in\ the\ essential\ oil)} * 100 \quad (1)$$

Loading Capacity

Loading capacity (% LC) measures the amount of EO loaded into the NLCs per unit mass of the lipid matrix. Since EO is a mixture of many compounds, a marker compound was chosen to quantify and indicate the approximate amount of loaded EO into NLCs.

A total of 1 mL of the NLC suspension was placed in a 2 mL Eppendorf tube. The NLCs were separated from the suspension medium via centrifugation at 14,000 rpm at 4 °C for 60 min, forming a pellet at the top due to the density difference between the NLCs and the aqueous medium. The supernatant was removed, and the pellet was washed with ethanol to eliminate any residual unencapsulated EO. The pellet was dried at room temperature to remove solvent residues. The dry weight of the NLC pellet was determined using an analytical balance. The dry pellet was transferred to a 2 mL Eppendorf tube, and 1 mL of chloroform was added. The mixture was sonicated and heated to 45 °C for 10 min in a sonication bath to dissolve the nanoparticles and extract the total EO present in the NLCs. Subsequently, centrifugation at 14,000 rpm for 30 min at 4 °C was performed to separate the wax from the chloroform, and the organic phase was removed from the Eppendorf tube. The amount of marker compound in the NLCs was quantified by GC. The loading capacity of EO in the NLCs was calculated using Equation (2) as the weight ratio of the marker to the NLCs, expressed as a percentage.

$$\%LC = \frac{(extracted\ marker\ compound\ mass)}{(NLC\ mass)} * 100 \quad (2)$$

2.6.4. Thermal Analysis

Differential scanning calorimetry (DSC) and thermogravimetric analysis (TGA) analyses were performed to study the thermal properties and phase transitions of the solid lipid matrix, yielding valuable insights into its stability and behavior under varying temperatures.

For sample preparation, 1 mL of the NLC suspension was placed in an Eppendorf tube. Centrifugation at 14,000 rpm at 4 °C for 1 h separated the NLCs from the suspension medium, forming a pellet at the top. The supernatant was removed, and the pellet was washed with ethanol to eliminate any residual unencapsulated EO, then dried at room temperature to remove solvent residues.

DSC analysis was conducted using a DSC 250 (TA Instrument, New Castle, DE, USA). Samples were heated at 5 °C/min from room temperature (26 °C) to 120 °C in a nitrogen atmosphere with a flow of 50 mL/min.

TGA analysis was performed with a TGA/DTA 5500 (TA Instrument, New Castle, DE, USA). Heating was carried out from room temperature (26 °C) to 600 °C at 5 °C/min in a nitrogen atmosphere with a flow of 50 mL/min, using a platinum sample holder.

2.7. Toxicity Test by Direct Contact

Bean plants were grown and maintained free of pesticides. Cultures of *M. persicae*, *T. urticae*, and *F. occidentalis* were maintained in laboratory conditions (25 ± 5 °C, 70 ± 5% RH). Circular leaf disks (4 cm diameter) were cut from healthy bean plants. Each disk was placed in a separate plastic container (8 cm diameter) with a pre-perforated lid and a veil to allow ventilation. Twenty adults of *M. persicae* and *T. urticae*, and ten adults of *F. occidentalis* were used per treatment. Each treatment was replicated four times.

Prior to treatment application, insects were gently transferred onto the leaf disks within the prepared containers. Treatment solutions were prepared as described in Table

S3, and 0.50 mL of each test solution were applied to the insects using a hand sprayer. Containers were maintained in laboratory conditions (25 ± 5 °C, 70 ± 5% RH).

Control groups included acetone (as solvent for EO dilutions), distilled water (as negative control), and CapsiAlil EC® insecticide at the recommended label concentration (as a positive control).

Mortality was recorded at 24 and 48 h post-treatment. Percentage mortality was calculated for each replicate. Data were analyzed using non-parametric methods (Kruskal-Wallis test, $\alpha = 0.05$). The results were analyzed by ANOVA using R (R 4.1.3, R Core Team, 2022).

3. Results

3.1. Chemical Composition of Essential Oils and Identification of Chemotypes

Table 2 shows TEO contains approximately equal proportions of oxygenated monoterpenes (47.5%) and monoterpene hydrocarbons (48.3%), with a low content of sesquiterpene hydrocarbons (4.2%). The predominant compound in the EO is thymol (35.6%), while all other components are below 19%. The monoterpene hydrocarbons in thyme oil are primarily γ-terpinene (18.7%) and p-cymene (18.1%), which serve as precursors to thymol and carvacrol [20]. Other significant constituents include linalool (3.1%), borneol (2.0%), carvacrol (1.5%), and terpinen-4-ol (1.1%). The chromatogram can be seen in Figure S1 (Supplementary data).

Table 2. Identification, retention times (t_R), and relative amounts (%) of the volatile fraction components present in the sample of essential oil from *T. vulgaris* analyzed by GC/MS (full scan).

t_R (min)	Chemical Compounds	Relative Amount (%)
9.5	Methyl 2-methylbutanoate	0.2
15.9	α-Thujene	2.2
16.3	α-Pinene	1.4
17.0	Camphene	1.0
18.0	Sabinene	0.1
18.2	Oct-1-en-3-ol	1.1
18.6	β-Myrcene	2.2
19.5	α-Phellandrene	0.3
19.6	Δ3-Carene	0.1
19.9	α-Terpinene	3.3
20.3	p-Cymene	18.1
20.5	Limonene	0.5
20.6	β-Phellandrene	0.2
20.6	1,8-Cineole	1.0
21.7	γ-Terpinene	18.7
21.8	Pent-4-en-1-yl butanoate	0.2
22.2	cis-Sabinene hydrate	0.4
22.8	Terpinolene	0.2
23.3	Linalool	3.1
23.5	trans-Sabinene hydrate	0.2
25.4	trans-Chrysanthemal	0.1
26.4	Borneol	2.0
26.7	Terpinen-4-ol	1.1
27.2	α-Terpineol	0.2
28.7	Thymyl methyl ether	0.1
28.8	Neral	0.2
29.9	Geranial	0.2
30.6	Thymol	35.6
30.7	Borneol acetate	0.3
30.9	Carvacrol	1.5
35.7	trans-β-Caryophyllene	4.0
38.8	γ-Cadinene	0.2

Table 3 indicates that REO has a higher content of monoterpene hydrocarbons (49.7%) compared to oxygenated monoterpenes (46.2%), with a low content of sesquiterpene hydrocarbons (4.1%). The chromatogram enables to identify α-pinene (19.4%) as the major compound, followed closely by 1,8-cineole, which is reported to have a higher relative amount (21.9%) than α-pinene. However, this is due to the combined relative area with β-phellandrene, as the substantial presence of 1,8-cineole caused peak overlap, hindering adequate resolution in this sample. As shown in the chromatogram, the peak intensity for 1,8-cineole was lower than that for α-pinene (see Figure S2 in Supplementary data). The third major compound was camphor (11.6%). Other significant compounds include camphene (7.6%), thymol (7.1%), γ-terpinene (4.4%), β-pinene (4.0%), β-caryophyllene (3.8%), limonene (3.7%), p-cymene (3.3%), and α-phellandrene (2.7%). These findings suggest that REO contains higher amounts of various monoterpenes, besides the three primary compounds that characterize each EO.

Table 3. Identification, retention times (t_R), and relative amounts (%) of the volatile fraction components present in the sample of essential oil from *R. officinalis* analyzed by GC/MS (full scan).

t_R (min)	Chemical Compounds	Relative Amount%
15.8	Tricyclene	0.3
15.9	α-Thujene	0.6
16.3	α-Pinene	19.4
17.1	Camphene	7.6
17.2	Thuja-2,4(10)-diene	0.1
18.3	β-Pinene	4.0
18.7	β-Myrcene	1.3
19.5	α-Phellandrene	2.7
19.9	α-Terpinene	1.4
20.3	p-Cymene	3.3
20.5	Limonene	3.7
20.7	1,8-Cineole + β-Phellandrene	21.9
21.7	γ-Terpinene	4.4
22.2	cis-Sabinene hydrate	0.2
22.8	Terpinolene	0.9
23.3	Linalool	0.6
23.5	trans-Sabinene hydrate	0.1
25.5	Camphor	11.6
26.4	Borneol	1.9
26.7	Terpinen-4-ol	0.7
27.2	α-Terpineol	0.8
27.7	Verbenone	1.1
30.5	Thymol	7.1
30.8	Carvacrol	0.2
35.7	trans-β-Caryophyllene	3.8
36.9	α-Humulene	0.3
15.8	Tricyclene	0.3
15.9	α-Thujene	0.6
16.3	α-Pinene	19.4
17.1	Camphene	7.6
17.2	Thuja-2,4(10)-diene	0.1
18.3	β-Pinene	4.0

3.2. Selection of NLC Preparation Method

The effect of the preparation method on the NLC properties was evaluated. Three top-down NLC preparation methods (HHPH, USH, and HSH) were evaluated.

To conserve resources, experiments were conducted using REO as a representative example. This decision was based on the premise that the relatively small size of monoterpenes, compared to lipids, suggests a potentially similar behavior within the formulation. REO-NLC were prepared using each method. For the REO-NLC, smaller particle sizes

were obtained with the HSH and HHPH methods, while larger sizes were obtained with the USH method. The particle sizes achieved by the HHPH method were the smallest among the three methods, but their PDI values were the highest (see Table 4). Particle size distributions of formulations produced by each method are shown in Figure 3. Zeta potential was more negative for NLCs produced by USH than the other two, but the zeta potential of NLCs produced by HSH was very close to −30 mV.

Table 4. Average particle size, polydispersity index and zeta potential of REO-NLC prepared by USH, HSH, and HHPH.

Formulation	Method	Particle Size (nm)	PDI	Zeta Potential (mV)
REO-NLC	USH	913.2 ± 37.5	0.205 ± 0.020	−43.8 ± 1.1
REO-NLC	HSH	505.1 ± 8.2	0.163 ± 0.027	−29.0 ± 0.6
REO-NLC	HHPH	285.8 ± 6.2	0.262 ± 0.019	−24.8 ± 0.5

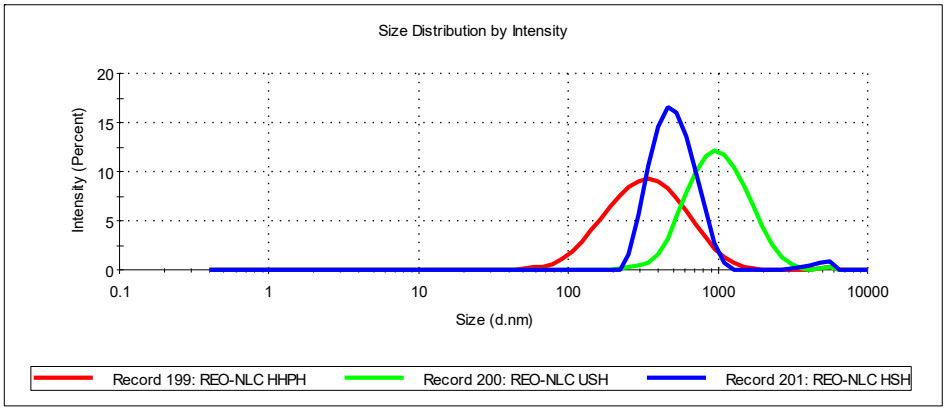

Figure 3. Particle size distributions of REO-NLC HHPH (red line); REO-NLC USH (green line); REO-NLC HSH (blue line).

Based on these results, it was decided to continue the preparation of the NLC using the HSH method, as it produces NLCs with sizes within the desired range and suitable zeta potential.

3.3. Factorial Design

A 2^3 factorial design with four replicates at the central point was conducted to investigate the effect of each excipient and their interactions in the colloidal properties of NLC dispersions. Experiments were conducted using REO as a representative example. Significant variables were identified through analysis of variance (ANOVA) at a 95% confidence level using R (R 4.1.3, R Core Team, 2022).

Table 5 shows that particle size ranged from 380 nm to 1432 nm. The minimum values for average size and PDI, and the maximum values for zeta potential, were obtained under the following conditions, 1% EO, 5% T80, and an LL:SL ratio of 25/75, resulting in a particle size of 453.1 nm, a PDI of 0.180, and a zeta potential of −37.1 mV, corresponding to NLC7 formulation.

Table 5. Average particle size, polydispersity index, and zeta potential of NLC formulations corresponding to the points of the factorial design.

Formulation	Particle Size (nm)	PDI	Zeta Potential (mV)
NLC1	644.7 ± 4.7	0.198 ± 0.036	−29.7 ± 0.7
NLC2	1432 ± 106	0.203 ± 0.103	−32.6 ± 0.3
NLC3	380.6 ± 24.3	0.566 ± 0.136	−55.1 ± 3.9
NLC4	1323 ± 150	0.505 ± 0.104	−30.8 ± 0.7
NLC5	555.2 ± 3.0	0.111 ± 0.066	−28.5 ± 0.4
NLC6	980.9 ± 34.7	0.707 ± 0.031	−21.9 ± 0.2
NLC7	453.1 ± 4.5	0.180 ± 0.030	−37.1 ± 0.7
NLC8	1075 ± 23.7	0.134 ± 0.024	−20.2 ± 0.3
NLC0	697.8 ± 34.1	0.193 ± 0.028	−39.8 ± 0.2
NLC0	590.6 ± 7.2	0.149 ± 0.019	−31.1 ± 1.0
NLC0	783.1 ± 27.7	0.141 ± 0.026	−46.1 ± 0.2
NLC0	897.5 ± 57.1	0.063 ± 0.023	−41.1 ± 0.5

The ANOVA of particle size revealed that the factors that significantly affected the particle size of REO-NLC were %EO, %T80, LL/SL, and the interaction %EO-LL/SL. This means that EO concentration, surfactant concentration, and LL/SL ratio had a linear effect and %EO-LL/SL was the main interaction. EO concentration significantly affected particle size ($p < 0.0001$). As the concentration of EO increased, the particle sizes tended to be larger. Surfactant concentration had a significant effect ($p < 0.05$) on particle size due to the reduction in surface tension. However, it is not the independent variable with the greatest effect on size changes, as both minimum and maximum levels result in smaller and larger particle sizes. The LL/SL ratio also had a significant effect ($p < 0.001$) on particle size, resulting in smaller sizes due to the reduction in the viscosity of the oil phase, which allowed the shear to be more effective in breaking the lipid mixture droplets (see Table S4).

At low EO concentration, the percentage of T80 significantly affected particle size ($p < 0.0001$) (see Table S7). Increasing the concentration of T80 led to a decrease in particle size due to reduction in interfacial tension between the two phases. However, at high EO concentrations, increasing the surfactant concentration did not have a statistically significant effect on particle size. Instead, at high EO concentrations the factor that significantly affects particle size is LL/SL ratio ($p < 0.001$) (see Table S8).

Regarding PDI, the ANOVA results showed that the factors that significantly affected PDI of REO-NLC were %EO, the interactions %EO-%T80, %EO-LL/SL, %T80-LL/SL, and the triple interaction %EO-%T80-LL/SL (see Table S5). At a low EO concentration, the PDI was affected by both the percentage of T80 ($p < 0.01$) and the LL/SL ratio ($p < 0.001$), as well as the interaction between these two factors ($p < 0.05$) (see Table S9). Increasing the surfactant concentration led to an increase in PDI. This is likely because excess surfactant can lead to the formation of micelles and smaller particles, which contribute to the increase in particle populations detected by the equipment. Additionally, an increase in surfactant concentration leads to higher PDI due to the excess surfactants bound to the particle surfaces [21,22].

The zeta potential ANOVA indicated that the factors that significantly affected zeta potential of REO-NLC were %EO, %T80, LL/SL, and the interaction %EO-%T80 (see Table S6). The higher the concentration of surfactant, the greater the absolute value of the zeta potential. This could be due to hydration of the polyethylene oxide (PEO) chains of T80. The water molecules would be accompanied by the ions in the system, contributing to the observed zeta potential values. On the other hand, an increase in the LL/SL ratio made the zeta potential less negative. It is important to note that carnauba wax contains 4% free fatty acids [23], and increasing the amount of Miglyol in the lipid phase decreases the proportion of free fatty acids on the particle surface, thus reducing the net negative charge of the particle.

The surface response charts and contour plots for the experimental design at low EO concentration and high EO concentration can be seen in Figure 4 The coefficients of the

response surface model for the three response variables at low and high EO concentrations are provided in the Supplementary Data.

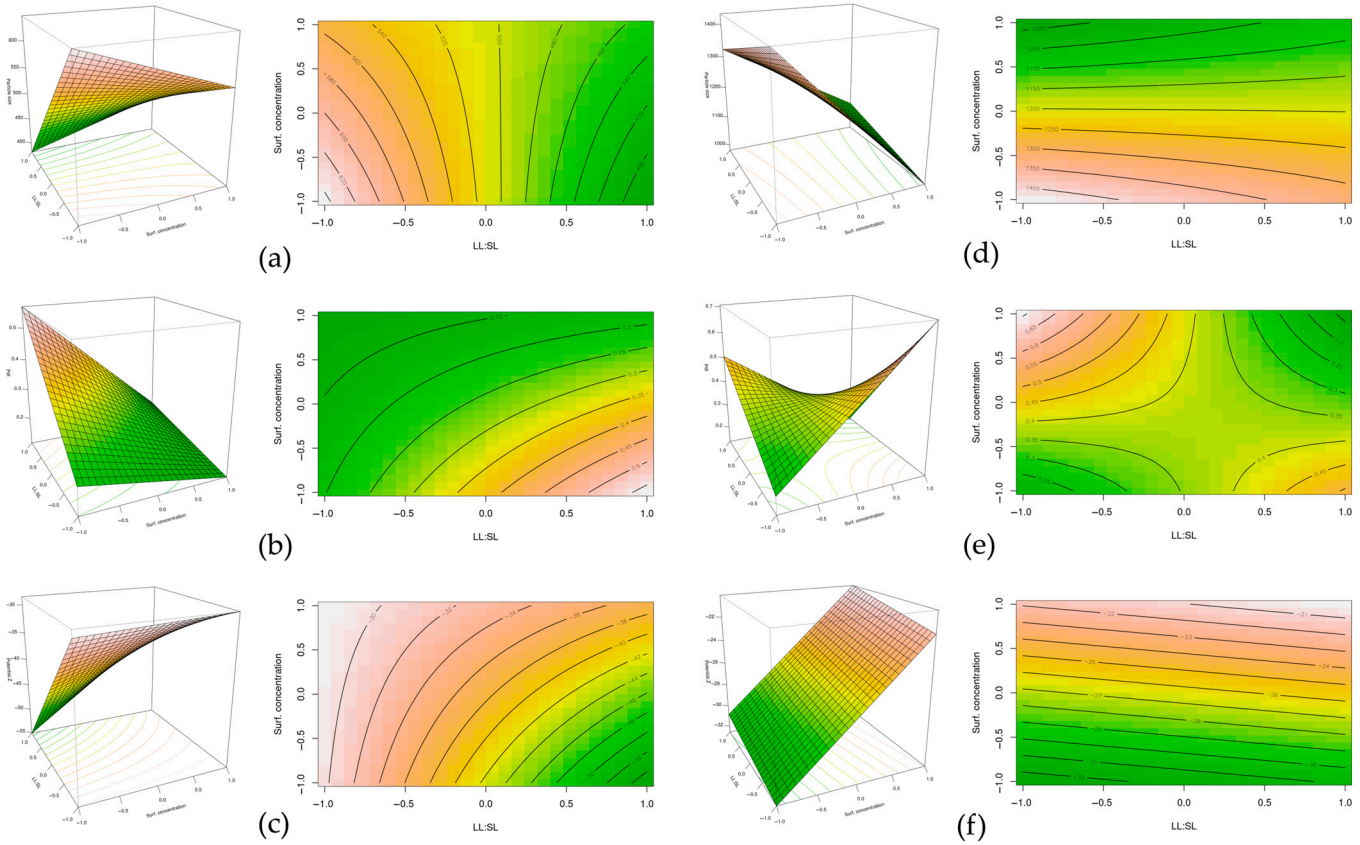

Figure 4. Surface response charts and contour plots of experimental design at EO low concentration: (**a**) particle size, (**b**) polydispersity index, and (**c**) zeta potential; and at EO high concentration: (**d**) particle size, (**e**) polydispersity index, and (**f**) zeta potential.

3.4. Determination of Morphology, Surface Characteristics, Internal Structure

Once the standard NLC formulation for both EOs was obtained, the morphology of the NLCs was analyzed via SEM and TEM. For this analysis, mean sizes between 288 and 353 nm, PDI between 0.153 and 0.188, and zeta potentials between −33.8 and −34.5 mV were obtained (see Table 6). The size distributions were narrow and monomodal (see Figure 5), and the particle sizes followed a trend REO-NLC < TEO-NLC < FEO-NLC (see Table 6).

Table 6. Average particle size, polydispersity index, and zeta potential of FEO-NLC, REO-NLC, and TEO-NLC.

Sample	Particle Size (nm)	PDI	Zeta Potential (mV)
FEO-NLC	352.9 ± 1.2	0.153 ± 0.019	−34.3 ± 0.7
TEO-NLC	347.8 ± 2.1	0.182 ± 0.015	−33.8 ± 0.4
REO-NLC	288.1 ± 1.7	0.188 ± 0.015	−34.5 ± 0.4

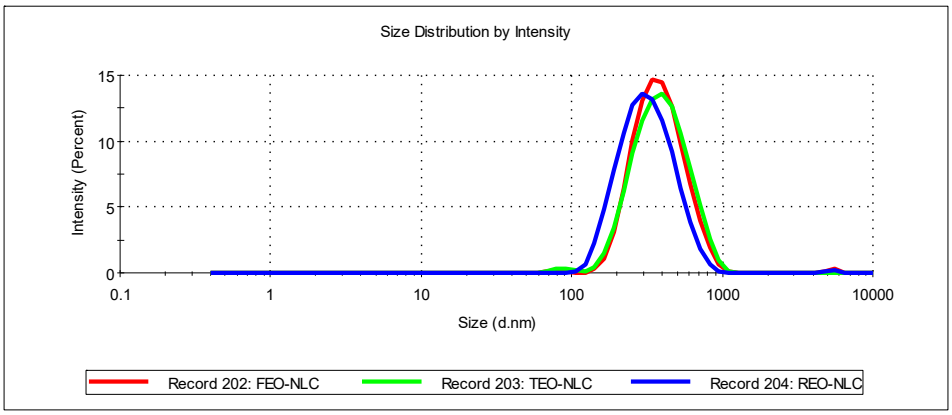

Figure 5. Particle size distributions of FEO-NLC (red line); TEO-NLC (green line); REO-NLC (blue line).

As can be seen in Figure 6 the images display almost spherical NLCs and particles sizes nearly to those ones obtained with DLS.

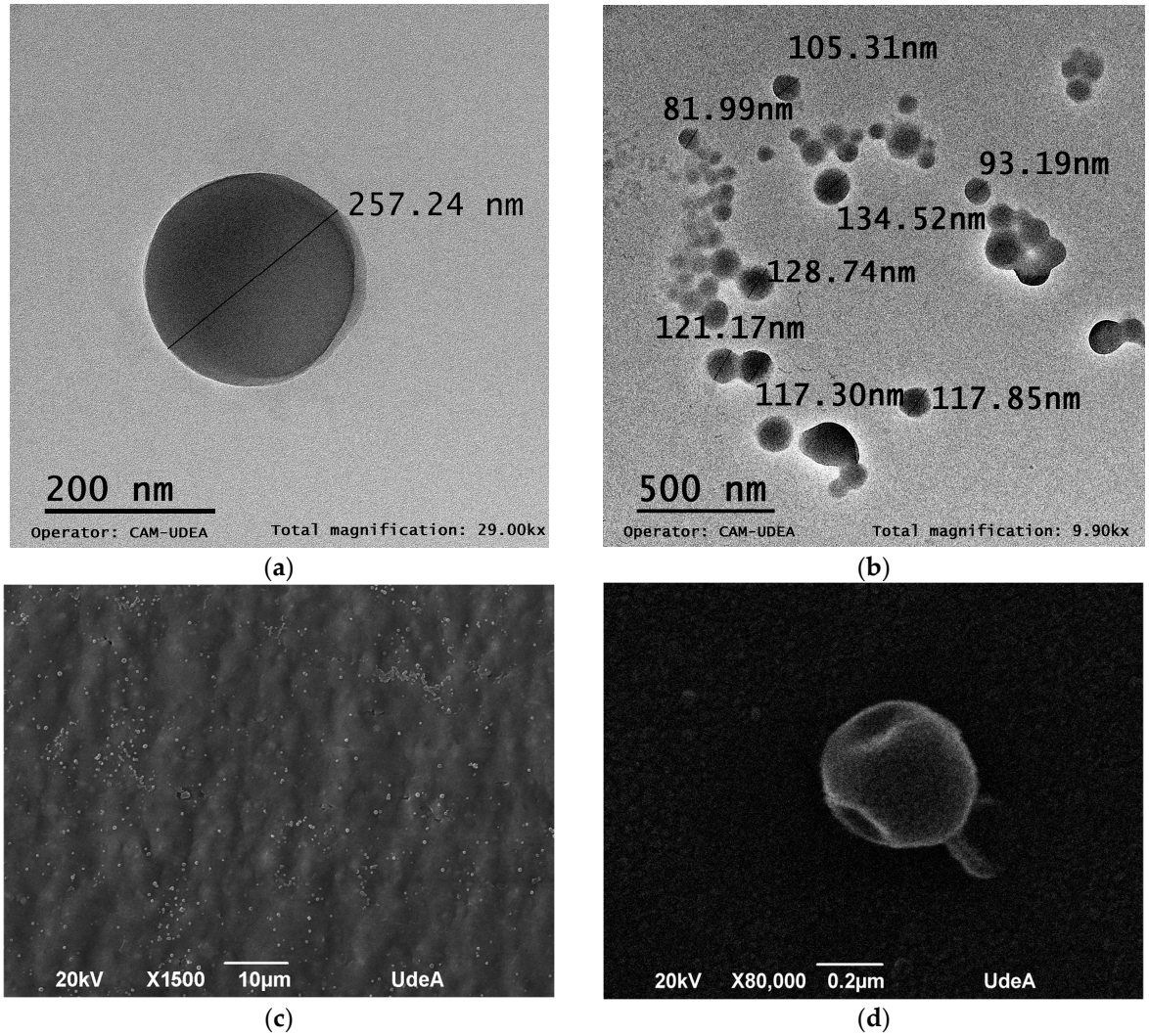

Figure 6. TEM and SEM images: (**a**) TEO-NLC TEM micrography; (**b**) REO-NLC TEM micrography; (**c**) TEO-NLC SEM micrography; (**d**) REO-NLC SEM micrography.

3.5. Encapsulation Efficiency and Loading Capacity

The marker compounds were quantified as an approximation to the amount of encapsulated EOs. The chromatograms of the total EO in the formulation and unencapsulated EO can also be seen (see Figures S3 and S4 in Supplementary Data).

As seen in Table 7, the encapsulation efficiency (%EE) and loading capacity (%LC) of the TEO-NLC formulations for the marker thymol were 71.9% and 1.18%, respectively. Similarly, the %EE and %LC of the REO-NLC formulations for the marker 1,8-cineole were 80.6% and 1.40%, respectively.

Table 7. EE (*w*/*w*, %) and LC (*w*/*w*,%) of the TEO-NLC and REO-NLC formulations.

Sample	Marker Compound	EE (%)	LC (%)
TEO-NLC	Thymol	71.9 ± 1.13	1.18 ± 0.21
REO-NLC	1,8-Cineole	80.6 ± 2.16	1.40 ± 0.43

3.6. DSC and TGA Analysis

To evaluate the thermal behavior and changes in the crystalline states of the NLCs, DSC and TGA were carried out. The results for the melting peak temperatures, onset and endset temperatures of melting as well as the enthalpies of melting, are presented in Table 8.

Table 8. DSC calorimetric parameters of CW, CW + MIG physical mixture, and NLC formulations.

Sample	Melting			
	Onset (°C)	Endset (°C)	Peak (T Melt, °C)	Enthalpy (J/g)
CW	71.05	85.77	82.79	187.32
CW + MIG	69.34	83.74	80.83	114.10
FEO-NLC	63.79	83.71	79.04	102.08
TEO-NLC	63.40	81.44	78.06	102.87
REO-NLC	65.30	83.10	79.65	117.96

All natural waxes have a complex composition and therefore do not have clearly defined melting points, as the classes of lipids contained have different melting ranges, which can also affect each other [24]. The melting peak temperature of CW was 82.79 °C with a melting enthalpy of 187.32 J/g. These results are close to those reported by several researchers due to the similarity of peaks [25,26]. However, these small differences are due to the variability in the purity of the starting materials [25]. The DSC curve for the melting of the CW-MIG physical mixture (Figure 7a, green line) shows the decrease in the melting temperature (80.83 °C) and the melting enthalpy (114.10 J/g) compared to CW DSC curve (Figure 7a, blue line). The DSC parameters for the FEO-NLCs shows that the melting temperature was 79.04 °C, and the melting enthalpy was 102.08 J/g. Similarly, the DSC parameters for TEO-NLCs and REO-NLCs show that the melting temperatures were 78.06 °C and 79.65, respectively, and the melting enthalpies were 102.87 J/g and 117.96 J/g, respectively.

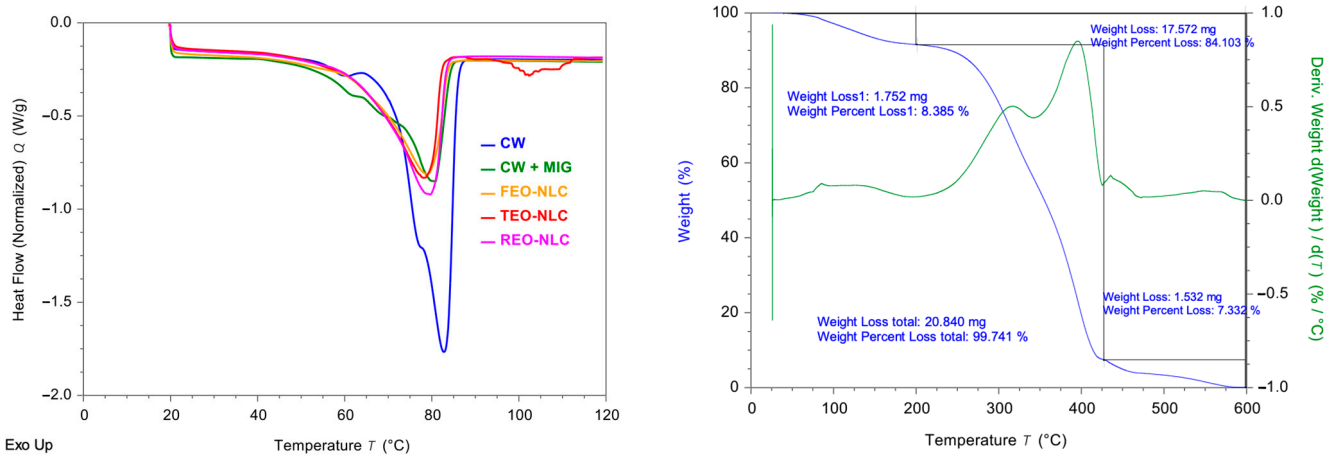

(**a**) (**b**)

Figure 7. DSC and TGA thermograms: (**a**) DSC curves: blue line for CW; green line for CW + MIG physical mixture; orange line for FEO-NLC; red line for TEO-NLC; pink line for REO-NLC; (**b**) TGA curve for NLC formulation with a TEO:REO 50:50 mixture.

Finally, the TG analysis of the EO-NLC sample (see Figure 7b) shows a mass loss between 56.15 and 199.49 °C, corresponding to 8.39% of the particle mass. This initial loss of 1.752 mg is related to the evaporation of the EO mass that is part of the particles. This result suggests that the system's loading capacity percentage may be around 8.39%. Between 199.49 °C and 427.20 °C, there is a mass loss of 17.57 mg, which is 84.1% of the sample mass. In this temperature range, both evaporation, decomposition, and phase transitions occur. Between 199.49 °C and 402 °C the triglycerides of capric and caprylic acids decompose and evaporate, along with the lower molecular weight compounds of the wax. Subsequently, the processes corresponding to the higher-molecular-weight compounds of the wax take place. Lastly, there is a weight loss of 1.532 mg, corresponding to 7.33% of the sample mass, which is likely related to the decomposition of Tween 80 and the remaining wax components.

3.7. Direct Contact Toxicity Assay

In this study, the contact toxic effect of different concentrations of EO solutions and EO-NLC suspensions on adults of *M. persicae*, *T. urticae*, and *F. occidentalis* was analyzed.

In Figure 8a, it can be observed that the treatments evaluated on *M. persicae* were notably ineffective on aphids, and no significant differences ($p = 0.1373$) were found between treatments. The highest mortality percentage (3.5%) was achieved with TEO at 1.5 mL/L. Mortality with the TEO-NLC formulation increased as the concentration increased from 1.0 mL/L to 1.5 mL/L.

In Figure 8b, it is shown that the highest mortality percentage (25%) in *T. urticae* was achieved with the FEO-NLC formulation at 1.5 mL/L. Additionally, no significant differences ($p = 0.1217$) were observed between treatments, as seen in supplementary data. The TEO-NLC formulation at 1.5 mL/L achieved a mortality rate close to 23%, while the REO-NLC at 1.5 mL/L reached mortality rates of 17%. It was expected that there would be a directly proportional relationship between the mortality rate and the increase in the concentration of the formulations; however, it was not possible to establish a clear relationship between the response variable and the concentrations of the formulations. For the treatments TEO-NLC and FEO-NLC, the mortality rate at the concentration of 1.0 mL/L was always below that corresponding to the concentrations of 0.5 mL/L and 1.5 mL/L. Only for the REO-NLC formulation and TEO was there an increased response as the concentration increased from 0.5 to 1.5 mL/L. With TEO, a mortality rate of 14% was achieved at 1.5 mL/L.

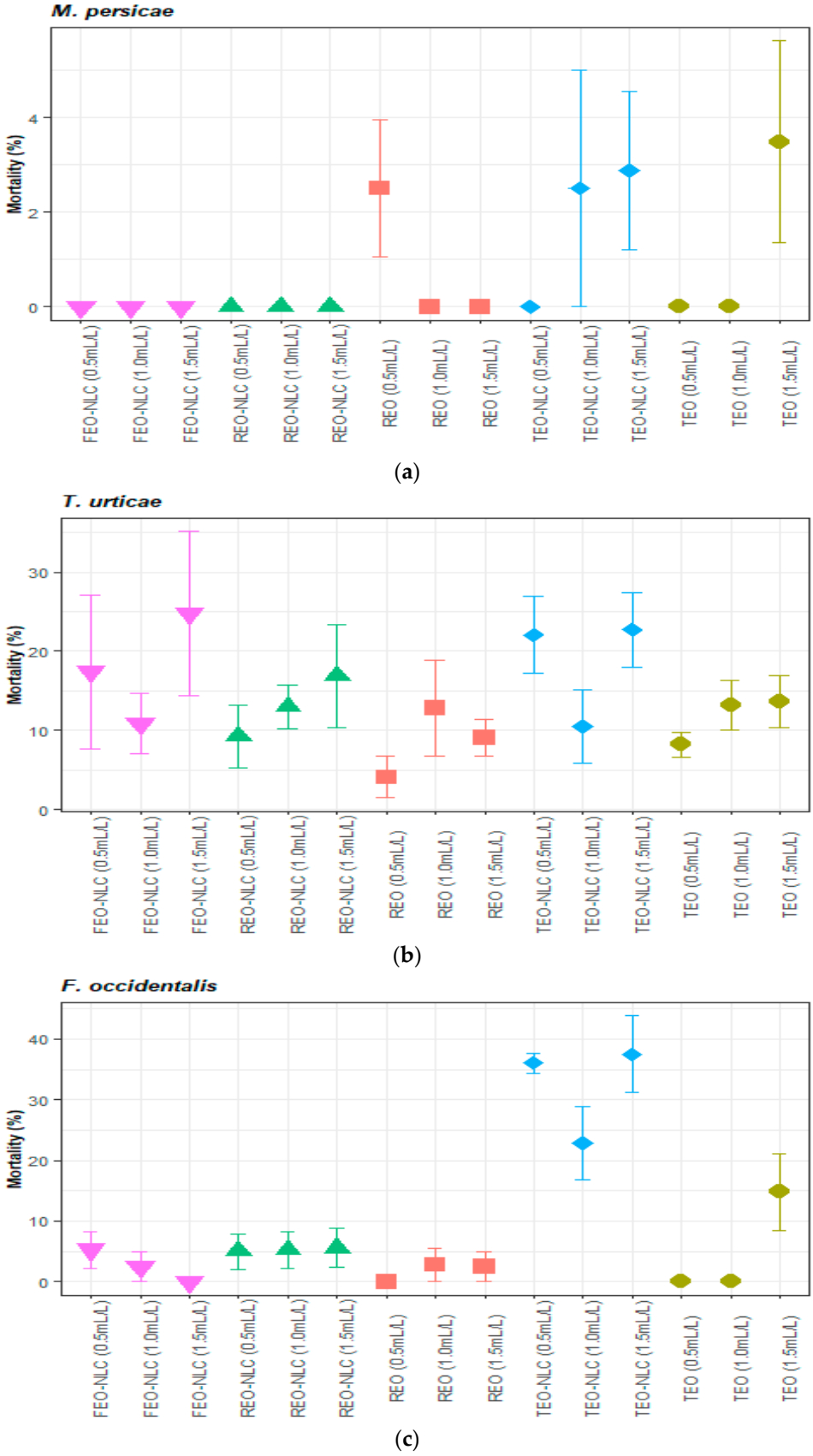

Figure 8. Mortality percentage of solutions of EOs and suspensions of EO-NLC: FEO-NLC (pink triangles), REO-NLC (green triangles), REO (red rectangles), TEO-NLC (blue rhombuses), and TEO on (green octahedron) (**a**) *M. persicae*, (**b**) *T. urticae*, and (**c**) *F. occidentalis*.

Regarding the test conducted on *F. occidentalis*, it can be observed in Figure 8c. that treatments with different concentrations of TEO-NLC achieved mortality rates between 24% and 38%, the highest obtained in this test for all insects, and these had significant differences ($p < 0.0001$) compared to other treatments.

4. Discussion

This study investigated the biopesticide potential of EO-NLC to address the need for safer pest control alternatives. We focused on developing and characterizing NLCs loaded with thyme and rosemary essential oils to improve these biopesticides' efficacy. Recognizing the influence of plant chemotypes on bioactivity, our study focused on specific chemotypes of thyme and rosemary for managing pests in ornamental flower production.

GC-MS analysis revealed that the essential oils extracted from thyme and rosemary, identified as the thymol chemotype and α-pinene chemotype, respectively, correspond to chemotypes with moderate to high biological activity reported against plant pests and pathogens [27–32]. In Pavela et al.'s [28] study, the essential oil of *Thymus vulgaris* demonstrated significant larvicidal and pupal mortality effects on the cotton leafworm (*Spodoptera littoralis*). When applied at sublethal doses, it caused total mortality of over 70% during the larval and pupal stages, making it one of the most effective oils tested. The primary bioactive compounds in TEO are thymol (68%) and carvacrol (12%), both phenolic compounds known for their potent insecticidal properties. Chemotype thymol is favored for its strong antibacterial properties, although its major compounds can be irritating. Industries such as pharmaceuticals and food manufacturing prioritize chemotypes thymol due to their desirable antimicrobial properties [33]. On the other hand, in the study by Khani and coworkers [30], the essential oil of *Rosmarinus officinalis* exhibited significant fumigant toxicity and repellent activity against the rice weevil (*Sitophilus oryzae*). The primary components of the REO included α-pinene (23.52%), verbenone (11.87%), and 1,8-cineole (8.56%), which contributed to its insecticidal effects. The study found that the LC50 (lethal concentration for 50% mortality) for REO was 115.63 µL/L of air, making it moderately toxic compared to other essential oils tested. Moreover, REO displayed strong repellent activity, with a 91% repellency rate at the highest concentration tested (16 µL/30 cm^2). In contrast, chemotype α-pinene may be preferred for its preservative properties in the food industry [34,35]. The main components of both EO have also demonstrated insecticidal and antimicrobial activity [36–41]. In our study, the extracted EOs were then incorporated into NLCs.

The preparation methods employed were HHPH, HSH, and USH. The results showed that HHPH was able to yield NLC with smaller particle sizes (285.8 nm), but it was the method with the broader size distribution (PDI: 0.262), and the less negative zeta potential (−24.8 mV). Moreover, it was a process that required a longer time preparation. Whereas USH produced the NLCs with the larger particle size (913.2 nm), a PDI in the optimal range (0.205), and the most negative zeta potential (−43 mV). In contrast, HSH was found to produce NLCs with a narrower size distribution. The HSH method proved effective in producing NLCs in the submicron range of 505 nm, with a PDI of 0.163 and zeta potential of −29.0 mV, suggesting good physical stability. These findings are consistent with previous studies reporting the efficiency of the HSH method for producing NLCs with controlled particle size and good stability [42].

While previous studies utilizing the HSH method for NLC production had achieved submicron particle sizes, polydispersity indices (>0.3) often indicated less than ideal stability [17,43,44]. In contrast, our study demonstrates that careful optimization of the HSH method can yield NLCs with not only submicron particle sizes but also polydispersity indices and zeta potentials, indicative of a highly stable system. Additionally, according to several authors, increasing the lipid content by more than 10% usually leads to larger particles, including microparticles, and broader particle size distributions [45,46]. However, it is important to note that in our study, we used a 20% lipid content and achieved relatively small sizes and narrow particle size distributions.

The formulation and optimization of NLCs in this study were guided by a factorial design approach. This approach allowed for the systematic evaluation of critical formulation parameters, including EO concentration, surfactant concentration, and the liquid-to-solid lipid ratio. By employing a factorial design, we were able to identify significant interactions between these variables and optimize key outcomes such as particle size, PDI, and zeta potential.

The 2^3 factorial design results showed that EO concentration, surfactant concentration, and liquid lipid/solid lipid ratio affected the colloidal properties of NLC formulation. The three factors analyzed had significant effects ($p < 0.05$) on the three response variables, except for the PDI, where the amount of surfactant and the LL/SL ratio did not have a significant effect. However, their interactions did show effects.

It is crucial to consider the concentration of EO in the liquid lipid/solid lipid (LL/SL) ratio. Higher EO concentrations resulted in larger particle sizes due to the reduced presence of Miglyol as the liquid lipid. This effect was evident in formulation NLC2 and NLC4, where the MIG/EO ratio was 0/100, resulting in the largest particle sizes. Similarly, formulations NLC6 and NLC8 with a MIG/EO ratio of 40/60 also showed relatively large particle sizes. In contrast, the smallest particle sizes were achieved with MIG/EO ratios of 66.7/33.3 in formulations NLC1 and NLC3, and 80/20 in formulations NLC5 and NLC7. Intermediate sizes were observed at the central points (NLC0) with a MIG/EO ratio of 50/50. The interaction between EO and LL/SL significantly impacted particle size, generally reducing it. Thus, maintaining a MIG/EO ratio of 50/50 or higher is recommended to achieve smaller particle sizes.

On the other hand, an increase in the LL/SL ratio has a negative effect on the PDI, meaning it decreases, which is desirable for the stability of the formulations. PDI values ranging from 0.1 to 0.25 suggest a relatively narrow size distribution, whereas a PDI values exceeding 0.5 signifies a very wide distribution [47]. This decrease is likely due to the reduction in the viscosity of the lipid phase, caused by an increase in liquid lipid content [48]. This reduction in viscosity makes it easier to break the structure of the lipid phase and form more homogeneous droplets. The interaction between LL/SL and %T80 also has a negative effect on the PDI, which aligns with the fact that decreasing the viscosity of the lipid phase and facilitating droplet formation allows the surfactant to play its key role in reducing interfacial tension, stabilizing the droplets, and covering the newly formed surfaces [45].

Encapsulation efficiency (%EE) values were 71.9% for thymol in TEO-NLC and 80.6% for 1,8-cineole in REO-NLC, demonstrating effective encapsulation of the EOs within the lipid matrix. Loading capacity (%LC) was also notable, reaching 1.18% in TEO-NLC and 1.40% in REO-NLC. EE% values suggest that CW-MIGLYOL-based NLCs can effectively encapsulate TEO and REO. Chromatograms comparing EOs extracted from NLC formulation to unencapsulated EOs support this. Figures S3 and S4 in the supplementary data present the chromatograms of unencapsulated EOs and NLC-encapsulated EOs, confirming the suitability of thymol and 1,8-cineole as indexed markers. These results are comparable to those obtained by Zhao et al. [42], where NLCs efficiently encapsulated *Houttuynia cordata* EO and yielded EE of 90.2%, 88.3%, and 76.6%, quantifying the content of 2-undecanone as the indexed marker. Similar results were obtained by Nasseri et al. [49] and Baldim and coworkers [50], with %EE for thymol of 84% and 90%, respectively. On the other hand, Shi et al. [51] determined the encapsulation efficiency using two marker compounds, such as β-elemene and octyl acetate. Their results were 77.9% and 88.2%, respectively. However, the loading capacity was much higher, with a value of 53.7%. Unfortunately, how it was calculated is not discussed. The other results were those reported by Miranda et al. [52], who obtained EE of 100% and LC of 1.40% of the total oil of *Ridolfia segetum*. The high encapsulation efficiency and loading capacity observed in our formulations are attributed to the incorporation of liquid lipids, which increase the imperfections in the lipid phase and improve the retention of bioactive compounds, as described in the literature on imperfect NLCs [47]. However, it is important to recognize that using a single compound as an

indexed marker does not provide a comprehensive assessment of the EE% and LC% of NLCs, as EOs consist of hundreds of components with varying molecular structures [42].

The morphology of NLCs reveals that the nanoparticles are spherical (Figure 6a,b) and uniform (Figure 6b,c), with an average size of approximately 200 nm (Figure 6a,b), which is slightly smaller than the size obtained through DLS measurements (around 350 nm) (see Table 6), although the apparent size by DLS will always be slightly larger due to the hydrodynamic radius, which is what the equipment ultimately detects and is not detected by TEM or SEM because the particles are dry. The unimodal distributions in Figure 5 indicate that HSH method generates NLC formulations with a narrow size distribution.

Thermal analysis indicated that the melting point of CW was 82.79 °C, with onset and endset temperatures at 71.05 °C and 85.77 °C, respectively. These findings are in agreement with prior studies [25]. In the DSC thermogram for the melting of carnauba wax (see Figure 7a, blue line), two solid–solid transitions can be observed: one at 56.71 °C and another at 77.5 °C. The first transition occurs before the melting begins and the second when it has already started, as highlighted by Basson and Reynhardt [53] and Reynhardt and Riederer [54]. The first solid–solid transition has been related to specific types of disorder in the orientation of the long hydrocarbon chains. The second solid–solid transition is due to the transition of lipids from an orthorhombic phase to a hexagonal phase. All waxes have an orthorhombic crystalline fraction at temperatures below the hexagonal phase transition [54].

This phase transition of CW appears to be specifically related to the transition to the hexagonal phase of aliphatic esters and diesters of 4-hydroxy and 4-methoxycinnamic acids, as reported by Freitas and coworkers [55] in their work, in which they isolated these compounds and performed the corresponding DSC and TG analysis. The DSC of the purified diesters showed two peaks at temperatures lower than those of CW, specifically at 66.88 °C and 73.51 °C, which are very similar in shape to the CW peaks but narrower and more pronounced. According to Craig et al. [56], the sharpness and extent of the peak indicate a higher crystallinity of the matrix.

The DSC thermogram for the melting of the CW-MIG physical mixture (see Figure 7a, green line) shows the shift of the first solid–solid transition region to a temperature of 59.84 °C and its incorporation into the melting event. It also shows the integration of the second solid–solid transition into the entire melting curve. The addition of MCT to the CW caused the endothermic peaks to broaden and shift to lower temperatures, which was expected due to the good affinity between the components of the mixture. The MCT were adequately incorporated into the structure of the wax components, reducing their crystallinity. These findings are in agreement with Severino et al. [57], who found that the lipid mixtures exhibited a decrease in melting temperature, suggesting a higher level of disorder within the lipid crystal. They point out that the concentration of liquid lipid influences the reduction in onset temperature and melting peak. A less-structured matrix promotes the formation of additional voids within its structure. Consequently, it can hold a greater amount of active ingredients, reducing the likelihood of expulsion during storage and also regulating the release [57].

The DSC thermogram of the TEO-NLC (see Figure 7a, red line) shows a distortion at the end of the heating curve, occurring after the lipid phase has completed melting. This finding is consistent with the results reported by Pires et al. [58], who studied NLC formulations loaded with thymol. In their research, thymol was observed to melt at 50.9 °C, and a strong interaction between Tween 80 and thymol caused the melting peak to shift to higher temperatures. This shift was attributed to the multiple proton acceptors in the molecular structure of Tween 80, which can form hydrogen bonds with the proton donor group of thymol. Such interactions increase the intermolecular forces, delaying the phase transition of the compound and raising its melting peak. Our results similarly suggest that significant amounts of thymol interact with the PEO chains of Tween 80 on the nanoparticle surface, preventing its immediate evaporation and contributing to the distortion observed in the DSC thermogram. It has been observed that lipid nanoparticle formulations containing

liquid lipids show a semicrystalline, less ordered, or amorphous structure compared to bulk waxes. In this sense, the presence of a liquid lipid and EO in the formulation decreases the crystallinity of the lipid phase, improving the encapsulation efficiency of the active principles. In other words, the use of liquid lipids increases the number of imperfections, which leads to a higher loading capacity and retention of bioactive compounds, likely giving rise to the first known model of NLCs called the imperfect type [59].

The mortality percentage was measured to evaluate the contact toxicity potential of crude and nanoencapsulated EOs of *T. vulgaris* and *R. officinalis* on *M. persicae*, *T. urticae*, and *F. occidentalis*.

REO, TEO, and their NLC formulations were preliminarily assessed for their potential insecticidal activity against thrips, aphids, and mites through contact application. Dose–response tests were conducted using direct contact assays, evaluating mortality rates over a 48 h period. TEO-NLCs demonstrated moderate contact toxicity, resulting in 38% mortality for *F. occidentalis*, with significant differences observed between treatments. This finding is consistent with previous studies reporting increased efficacy of nanoencapsulated EOs. For instance, Ibrahim et al. [60] found that garlic EO-SLN exhibited significantly higher mortality against *P. operculella* larvae compared to the free oil across various concentrations in laboratory conditions. Specifically, at concentrations of 0.625% and 1.25% of garlic EO-SLN resulted in 36% and 48% larval mortality, respectively, compared to significantly lower mortality rates observed for the free oil.

In the study conducted by Adel et al. [61], they investigated the efficacy of geranium EO, both in its free form and nanoencapsulated within SLN, against *A. ipsilon* larvae. Two oil concentrations (2.5% and 5.0%) were tested for both treatments, alongside a control group. Their findings demonstrated that nanoencapsulation significantly enhanced the insecticidal activity of geranium EO. Among the treatments, SLN loaded with 2.5% geranium EO effectively controlled *A. ipsilon* larvae, resulting in a 48% larval mortality rate, while SLNs loaded with 5.0% geranium EO exhibited the highest efficacy, causing a larval mortality of 60%.

In our study, REO-NLCs, TEO-NLCs, and FEO-NLCs caused mild mortality rates of 17%, 23%, and 25%, respectively, in *T. urticae*, although no significant differences were noted between treatments. Conversely, the NLC formulations had no impact on *M. persicae* mortality. The mortality observed with REO-NLC, TEO-NLC, and FEO-NLC can be explained by the inherent characteristics of the nanoparticles, which include occlusive and dehydrating effects. For example, Zayed et al. [62] demonstrated that silica nanoparticles enhanced the acaricidal activity of abamectin against *Tetranychus urticae.* Nanoparticles, due to their small size and high surface area, can form a film over the mite surface, leading to reduced gas and moisture exchange by obstruction of the mite's respiratory system. However, based on the findings of Sioutas et al. [63], nanoparticles do not necessarily cause mortality through dehydration. Their study on the acaricidal activity of silver nanoparticles (AgNPs) against *Dermanyssus gallinae,* the poultry red mite, showed that dehydration was not the primary mechanism of action. Instead, the AgNPs caused significant physical damage to the mites' exoskeleton by interacting with chitin, leading to cracks and fractures in the cuticle structure.

On the other hand, the mortality rate observed with FEO-NLC aligns with the findings of Tortorici et al. [64] for the aphid *A. gossypii*. Their biological tests revealed that the NLC blank formulation led to significant mortality and reduced offspring in *A. gossypii*. They suggest that the high mortality and decreased fertility in aphids might be attributed to the surfactants in the NLC blank formulation, which have been shown to disrupt cellular integrity and affect physiological processes in various insect species [65].

Similarly, in our study, TEO-NLC resulted in significantly higher *F. occidentalis* adult mortality rates compared to their free oil counterpart. The improved insecticidal activity can be attributed to the molecules of thymol interacting with the polyethylene oxide chains of Tween 80, acting as a trigger. Additionally, it can be attributed to the penetration

capacity of EOs when encapsulated in NLC, as they can remain on the surface of the insects' exoskeleton for a longer period and exert their toxic effect.

5. Conclusions

This study investigated the potential of thyme and rosemary EO-NLC as biopesticides against ornamental flower pests. High shear homogenization proved effective in producing NLCs with desirable physicochemical properties, including optimal particle size, particle size distribution, and zeta potential. Thyme EO-NLCs exhibited moderate contact toxicity against *Frankliniella occidentalis* and mild toxicity against *Tetranychus urticae*. Conversely, rosemary EO-NLCs showed minimal efficacy against the tested pests. This difference in insecticidal activity highlights the importance of EO chemical composition in biopesticide efficacy. The high thymol content in thyme EO likely contributed to its enhanced toxicity. These findings indicate that TEO-NLCs show potential as biopesticides for controlling specific pests of ornamental flowers. However, further research is needed to optimize the administration dosage, refine NLC formulations, evaluate their long-term efficacy and stability, and assess any potential impact on non-target organisms.

Supplementary Materials: The following supporting information can be downloaded at https://www.mdpi.com/article/10.3390/colloids8050055/s1: Table S1: The 2^3 factorial design combinations; Table S2: MIG/EO ratio in the NLC formulations of the factorial design; Table S3: Experimental design of contact toxicity test; Table S4: Coefficients of the model and ANOVA table for particle size; Table S5: Coefficients of the model and ANOVA table for PDI; Table S6: Coefficients of the model and ANOVA table for zeta potential; Table S6: Coefficients of the model and ANOVA table for zeta potential; Table S7: Coefficients of the response surface model for particle size at low EO concentration; Table S8: Coefficients of the response surface model for particle size at high EO concentration; Table S9: Coefficients of the response surface model for PDI at low EO concentration; Table S10: Coefficients of the response surface model for PDI at high EO concentration; Table S11: Coefficients of the response surface model for zeta potential at low EO concentration; Table S12: Coefficients of the response surface model for zeta potential at low EO concentration; Figure S1: Chromatogram of Thyme essential oil; Figure S2: Chromatogram of Rosemary essential oil; Figure S3: Chromatograms of (a) total rosemary essential oil extracted from the formulation and (b) unencapsulated rosemary essential oil; Figure S4: Chromatograms of (a) total compounds of thyme essential oil extracted from the formulation and (b) unencapsulated compounds of thyme essential oil.

Author Contributions: Conceptualization, A.M.-E. and F.S.-S.; methodology, A.M.-E. and F.S.-S.; software, J.L.M.-E.; validation, F.S.-S.; formal analysis, A.M.-E. and F.S.-S.; investigation, A.M.-E. and F.S.-S.; resources, A.M.-E. and F.S.-S.; data curation, J.L.M.-E.; writing—original draft preparation, A.M.-E.; writing—review and editing, F.S.-S. and J.L.M.-E.; supervision, F.S.-S.; project administration, F.S.-S.; funding acquisition, A.M.-E. All authors have read and agreed to the published version of the manuscript.

Funding: This research was funded by MINCIENCIAS grant number 727 of 2015 for the formation of Colombian PhDs.

Data Availability Statement: The original contributions presented in the study are included in the article/supplementary material. Further inquiries can be directed to the corresponding authors.

Acknowledgments: The authors thank the Faculty of Pharmaceutical and Food Sciences for equipment loan for the development of the study.

Conflicts of Interest: Author Jose L. Múnera-Echeverri was employed by the company Ecofresca S.A.S. The remaining authors declare that the research was conducted in the absence of any commercial or financial relationships that could be construed as a potential conflict of interest.

References

1. Rani, N.; Duhan, A.; Pal, A.; Kumari, P.; Beniwal, R.K.; Verma, D.; Goyat, A.; Singh, R. Are Nano-Pesticides Really Meant for Cleaner Production? An Overview on Recent Developments, Benefits, Environmental Hazards and Future Prospectives. *J. Clean. Prod.* **2023**, *411*, 137232. [CrossRef]

2. Swain, S.S.; Paidesetty, S.K.; Padhy, R.N.; Hussain, T. Nano-Technology Platforms to Increase the Antibacterial Drug Suitability of Essential Oils: A Drug Prospective Assessment. *OpenNano* **2023**, *9*, 100115. [CrossRef]
3. Rojas, K.; Verdugo-Molinares, M.G.; Vallejo-Cardona, A.A. Use of Encapsulating Polymers of Active Compounds in the Pharmaceutical and Food Industry. *Food Chem. Adv.* **2024**, *4*, 100619. [CrossRef]
4. Salvioni, L.; Morelli, L.; Ochoa, E.; Labra, M.; Fiandra, L.; Palugan, L.; Prosperi, D.; Colombo, M. The Emerging Role of Nanotechnology in Skincare. *Adv. Colloid Interface Sci.* **2021**, *293*, 102437. [CrossRef]
5. Garg, J.; Pathania, K.; Sah, S.P.; Pawar, S.V. Nanostructured Lipid Carriers: A Promising Drug Carrier for Targeting Brain Tumours. *Future J. Pharm. Sci.* **2022**, *8*, 25. [CrossRef]
6. Scioli Montoto, S.; Muraca, G.; Ruiz, M.E. Solid Lipid Nanoparticles for Drug Delivery: Pharmacological and Biopharmaceutical Aspects. *Front. Mol. Biosci.* **2020**, *7*, 587997. [CrossRef]
7. Jugreet, B.S.; Suroowan, S.; Rengasamy, R.R.K.; Mahomoodally, M.F. Chemistry, Bioactivities, Mode of Action and Industrial Applications of Essential Oils. *Trends Food Sci. Technol.* **2020**, *101*, 89–105. [CrossRef]
8. Chaudhari, A.K.; Singh, V.K.; Kedia, A.; Das, S.; Dubey, N.K. Essential Oils and Their Bioactive Compounds as Eco-Friendly Novel Green Pesticides for Management of Storage Insect Pests: Prospects and Retrospects. *Environ. Sci. Pollut. Res.* **2021**, *28*, 18918–18940. [CrossRef]
9. Raveau, R.; Fontaine, J.; Lounès-Hadj Sahraoui, A. Essential Oils as Potential Alternative Biocontrol Products against Plant Pathogens and Weeds: A Review. *Foods* **2020**, *9*, 365. [CrossRef]
10. Katopodi, A.; Detsi, A. Solid Lipid Nanoparticles and Nanostructured Lipid Carriers of Natural Products as Promising Systems for Their Bioactivity Enhancement: The Case of Essential Oils and Flavonoids. *Colloids Surf. A Physicochem. Eng. Asp.* **2021**, *630*, 127529. [CrossRef]
11. Cimino, C.; Maurel, O.M.; Musumeci, T.; Bonaccorso, A.; Drago, F.; Souto, E.M.B.; Pignatello, R.; Carbone, C. Essential Oils: Pharmaceutical Applications and Encapsulation Strategies into Lipid-Based Delivery Systems. *Pharmaceutics* **2021**, *13*, 327. [CrossRef] [PubMed]
12. Kumar, A.; Kanwar, R.; Mehta, S.K. Recent Development in Essential Oil-Based Nanocarriers for Eco-Friendly and Sustainable Agri-Food Applications: A Review. *ACS Agric. Sci. Technol.* **2022**, *2*, 823–837. [CrossRef]
13. Pereira, P.C.G.; Parente, C.E.T.; Carvalho, G.O.; Torres, J.P.M.; Meire, R.O.; Dorneles, P.R.; Malm, O. A Review on Pesticides in Flower Production: A Push to Reduce Human Exposure and Environmental Contamination. *Environ. Pollut.* **2021**, *289*, 117817. [CrossRef] [PubMed]
14. McGovern, R.J.; Elmer, W.H. Florists' Crops: Global Trends and Disease Impact. In *Handbook of Florists' Crops Diseases*; McGovern, R.J., Elmer, W.H., Eds.; Springer: Berlin/Heidelberg, Germany, 2018; pp. 1–9.
15. Silva-Castaño, A.F.; Brochero, H.L. Abundance and Flight Activity of *Frankliniella occidentalis* (Thysanoptera: Thripidae) in a Female Chrysanthemum Crop for Seeding, Colombia. *Agron. Colomb.* **2021**, *39*, 216–225. [CrossRef]
16. Molina-Acosta, M.D.; Calvo, S.J.; Palacio, M.M.; Giraldo, C.E. Incidencia de plagas en material poscosecha de nueve cultivares de hortensia tipo exportación, en Antioquia (Colombia). *Rev. Colomb. Entomol.* **2021**, *47*, e7530. [CrossRef]
17. Khezri, K.; Farahpour, M.R.; Mounesi Rad, S. Accelerated Infected Wound Healing by Topical Application of Encapsulated Rosemary Essential Oil into Nanostructured Lipid Carriers. *Artif. Cells Nanomed. Biotechnol.* **2019**, *47*, 980–988. [CrossRef]
18. Souto, E.B.; Severino, P.; Marques, C.; Andrade, L.N.; Durazzo, A.; Lucarini, M.; Atanasov, A.G.; El Maimouni, S.; Novellino, E.; Santini, A. *Croton argyrophyllus* Kunth Essential Oil-Loaded Solid Lipid Nanoparticles: Evaluation of Release Profile, Antioxidant Activity and Cytotoxicity in a Neuroblastoma Cell Line. *Sustainability* **2020**, *12*, 7697. [CrossRef]
19. Baldim, I.; Tonani, L.; Von Zeska Kress, M.R.; Pereira Oliveira, W. *Lippia sidoides* Essential Oil Encapsulated in Lipid Nanosystem as an Anti-Candida Agent. *Ind. Crops Prod.* **2019**, *127*, 73–81. [CrossRef]
20. Stahl-Biskup, E. Essential Oil Chemistry of the Genus Thymus—A Global View. In *Thyme*; CRC Press: Boca Raton, FL, USA, 2002.
21. Ferreira, M.; Chaves, L.L.; Lima, S.A.C.; Reis, S. Optimization of Nanostructured Lipid Carriers Loaded with Methotrexate: A Tool for Inflammatory and Cancer Therapy. *Int. J. Pharm.* **2015**, *492*, 65–72. [CrossRef]
22. Das Neves, J.; Sarmento, B. Precise Engineering of Dapivirine-Loaded Nanoparticles for the Development of Anti-HIV Vaginal Microbicides. *Acta Biomater.* **2015**, *18*, 77–87. [CrossRef]
23. Krendlinger, E.J.; Wolfmeier, U.H. (Eds.) Carnauba Wax. In *Natural and Synthetic Waxes Origin, Production, Technology, and Applications*; Wiley-VCH: Weinheim, Germany, 2023; pp. 129–152.
24. Ritter, B.; Schulte, J.; Schulte, E.; Thier, H.P. Detection of Coating Waxes on Apples by Differential Scanning Calorimetry. *Eur. Food Res. Technol.* **2001**, *212*, 603–607. [CrossRef]
25. Öğütcü, M.; Yilmaz, E. Characterization of Hazelnut Oil Oleogels Prepared with Sunflower and Carnauba Waxes. *Int. J. Food Prop.* **2015**, *18*, 1741–1755. [CrossRef]
26. Yi, B.R.; Kim, M.J.; Lee, S.Y.; Lee, J.H. Physicochemical Properties and Oxidative Stability of Oleogels Made of Carnauba Wax with Canola Oil or Beeswax with Grapeseed Oil. *Food Sci. Biotechnol.* **2017**, *26*, 79–87. [CrossRef] [PubMed]
27. Khoobdel, M.; Ahsaei, S.M.; Farzaneh, M. Insecticidal Activity of Polycaprolactone Nanocapsules Loaded with *Rosmarinus Officinalis* Essential Oil in *Tribolium Castaneum* (Herbst). *Entomol. Res.* **2017**, *47*, 175–184. [CrossRef]
28. Pavela, R. Sublethal Effects of Some Essential Oils on the Cotton Leafworm Spodoptera Littoralis (Boisduval). *J. Essent. Oil Bear. Plants* **2012**, *15*, 144–156. [CrossRef]

29. Pavela, R. Insecticidal and Repellent Activity of Selected Essential Oils against of the Pollen Beetle, *Meligethes aeneus* (Fabricius) Adults. *Ind. Crops Prod.* **2011**, *34*, 888–892. [CrossRef]
30. Khani, M.; Marouf, A.; Amini, S.; Yazdani, D.; Farashiani, M.E.; Ahvazi, M.; Khalighi-Sigaroodi, F.; Hosseini-Gharalari, A. Efficacy of Three Herbal Essential Oils Against Rice Weevil, *Sitophilus Oryzae* (Coleoptera: Curculionidae). *J. Essent. Oil Bear. Plants* **2017**, *20*, 937–950. [CrossRef]
31. Soković, M.D.; Vukojević, J.; Marin, P.D.; Brkić, D.D.; Vajs, V.; Van Griensven, L.J.L.D. Chemical Composition of Essential Oils of Thymus and Mentha Speciesand Their Antifungal Activities. *Molecules* **2009**, *14*, 238–249. [CrossRef]
32. Pitarokili, D.; Tzakou, O.; Loukis, A. Composition of the Essential Oil of Spontaneous *Rosmarinus officinalis* from Greece and Antifungal Activity Against Phytopathogenic Fungi. *J. Essent. Oil Res.* **2008**, *20*, 457–459. [CrossRef]
33. Rey, C.; Sáez, F. Field Culture, in Vitro Culture and Selection of Thymus. In *Thyme The genus Thymtls*; Stahl-Biskup, E., Saez, F., Eds.; Taylor & Francis Group: Abingdon, UK, 2002; pp. 177–196.
34. Stashenko, E. Propiedades y Caracterización. In *Aceites Esenciales*; Stashenko, E.E., Ed.; Universidad Industrial de Santander: Bucaramanga, Colombia, 2009; pp. 85–124, ISBN 978-958-44-5944-2.
35. Ivanovic, J.; Misic, D.; Zizovic, I.; Ristic, M. In Vitro Control of Multiplication of Some Food-Associated Bacteria by Thyme, Rosemary and Sage Isolates. *Food Control* **2012**, *25*, 110–116. [CrossRef]
36. Miresmailli, S.; Bradbury, R.; Isman, M.B. Comparative Toxicity of *Rosmarinus officinalis* L. Essential Oil and Blends of Its Major Constituents against Tetranychus Urticae Koch (Acari: Tetranychidae) on Two Different Host Plants. *Pest Manag. Sci.* **2006**, *62*, 366. [CrossRef] [PubMed]
37. Langsi, J.D.; Nukenine, E.N.; Oumarou, K.M.; Moktar, H.; Fokunang, C.N.; Mbata, G.N. Evaluation of the Insecticidal Activities of α-Pinene and 3-Carene on *Sitophilus zeamais* Motschulsky (Coleoptera: Curculionidae). *Insects* **2020**, *11*, 540. [CrossRef] [PubMed]
38. Perina, F.J.; Amaral, D.C.; Fernandes, R.S.; Labory, C.R.; Teixeira, G.A.; Alves, E. *Thymus vulgaris* Essential Oil and Thymol against *Alternaria alternata* (Fr.) Keissler: Effects on Growth, Viability, Early Infection and Cellular Mode of Action: Thymol (2-Isopropyl-5-Methylphenol) for the Control of *Alternaria alternata*: Mode of Action. *Pest. Manag. Sci.* **2015**, *71*, 1371–1378. [CrossRef] [PubMed]
39. Ferreira, L.E. *Thymus vulgaris* L. Essential Oil and Its Main Component Thymol: Anthelmintic Effects against Haemonchus Contortus from Sheep. *Vet. Parasitol.* **2016**, *228*, 70–76. [CrossRef] [PubMed]
40. Abbaszadeh, S.; Sharifzadeh, A.; Shokri, H.; Khosravi, A.R.; Abbaszadeh, A. Antifungal Efficacy of Thymol, Carvacrol, Eugenol and Menthol as Alternative Agents to Control the Growth of Food-Relevant Fungi. *J. Mycol. Medicale* **2014**, *24*, e51–e56. [CrossRef]
41. Kordali, S.; Cakir, A.; Ozer, H.; Cakmakci, R.; Kesdek, M.; Mete, E. Antifungal, Phytotoxic and Insecticidal Properties of Essential Oil Isolated from Turkish Origanum Acutidens and Its Three Components, Carvacrol, Thymol and p-Cymene. *Bioresour. Technol.* **2008**, *99*, 8788–8795. [CrossRef]
42. Zhao, Y.; Chang, Y.X.; Hu, X.; Liu, C.Y.; Quan, L.H.; Liao, Y.H. Solid Lipid Nanoparticles for Sustained Pulmonary Delivery of Yuxingcao Essential Oil: Preparation, Characterization and in Vivo Evaluation. *Int. J. Pharm.* **2017**, *516*, 364–371. [CrossRef]
43. Souto, E.B.; Doktorovova, S.; Zielinska, A.; Silva, A.M. Key Production Parameters for the Development of Solid Lipid Nanoparticles by High Shear Homogenization. *Pharm. Dev. Technol.* **2019**, *24*, 1181–1185. [CrossRef]
44. Ghodrati, M.; Farahpour, M.R.; Hamishehkar, H. Encapsulation of Peppermint Essential Oil in Nanostructured Lipid Carriers: In-Vitro Antibacterial Activity and Accelerative Effect on Infected Wound Healing. *Colloids Surf. A Physicochem. Eng. Asp.* **2019**, *564*, 161–169. [CrossRef]
45. Mehnert, W.; Mader, K. Solid Lipid Nanoparticles Production, Characterization and Applications. *Adv. Drug Deliv. Rev.* **2001**, *47*, 165–196. [CrossRef]
46. Müller, R.H.; Radtke, M.; Wissing, S.A. Solid Lipid Nanoparticles (SLN) and Nanostructured Lipid Carriers (NLC) in Cosmetic and Dermatological Preparations. *Adv. Drug Deliv. Rev.* **2002**, *54*, 131–155. [CrossRef] [PubMed]
47. Tamjidi, F.; Shahedi, M.; Varshosaz, J.; Nasirpour, A. Nanostructured Lipid Carriers (NLC): A Potential Delivery System for Bioactive Food Molecules. *Innov. Food Sci. Emerg. Technol.* **2013**, *19*, 29–43. [CrossRef]
48. Zielińska, A.; Ferreira, N.R.; Durazzo, A.; Lucarini, M.; Cicero, N.; Mamouni, S.E.; Silva, A.M.; Nowak, I.; Santini, A.; Souto, E.B. Development and Optimization of Alpha-Pinene-Loaded Solid Lipid Nanoparticles (SLN) Using Experimental Factorial Design and Dispersion Analysis. *Molecules* **2019**, *24*, 2683. [CrossRef]
49. Nasseri, M.; Golmohammadzadeh, S.; Arouiee, H.; Jaafari, M.R.; Neamati, H. Antifungal Activity of *Zataria multiflora* Essential Oil-Loaded Solid Lipid Nanoparticles in-Vitro Condition. *Iran. J. Basic Med. Sci.* **2016**, *19*, 1231–1237. [CrossRef] [PubMed]
50. Baldim, I.; Paziani, M.H.; Grizante Barião, P.H.; von Zeska Kress, M.R.; Oliveira, W.P. Nanostructured Lipid Carriers Loaded with *Lippia sidoides* Essential Oil as a Strategy to Combat the Multidrug-Resistant *Candida auris*. *Pharmaceutics* **2022**, *14*, 180. [CrossRef]
51. Shi, F.; Zhao, J.-H.; Liu, Y.; Wang, Z.; Zhang, Y.-T.; Feng, N.-P. Preparation and Characterization of Solid Lipid Nanoparticles Loaded with Frankincense and Myrrh Oil. *Int. J. Nanomed.* **2012**, *7*, 2033–2043. [CrossRef]
52. Miranda, M.; Cruz, M.T.; Vitorino, C.; Cabral, C. Nanostructuring Lipid Carriers Using *Ridolfia segetum* (L.) Moris Essential Oil. *Mater. Sci. Eng. C* **2019**, *103*, 109804. [CrossRef]
53. Basson, I.; Reynhardt, E.C. An Investigation of the Structures and Molecular Dynamics of Natural Waxes II. Carnauba Wax. *J. Phys. D Appl.* **1988**, *21*, 1429–1433. [CrossRef]
54. Reynhardt, E.C.; Riederer, M. Structures and Molecular Dynamics of Plant Waxes. *Eur. Biophys. J.* **1994**, *23*, 59–70. [CrossRef]

55. Freitas, C.A.S.; Vieira, Í.G.P.; Sousa, P.H.M.; Muniz, C.R.; Gonzaga, M.L.D.C.; Guedes, M.I.F. Carnauba Wax P-Methoxycinnamic Diesters: Characterisation, Antioxidant Activity and Simulated Gastrointestinal Digestion Followed by in Vitro Bioaccessibility. *Food Chem.* **2016**, *196*, 1293–1300. [CrossRef]
56. Craig, R.G.; Eick, J.D.; Peyton, F.A. Properties of Natural Waxes Used in Dentistry. *J. Dent. Res.* **1965**, *44*, 1308–1316. [CrossRef]
57. Severino, P.; Pinho, S.C.; Souto, E.B.; Santana, M.H.A. Polymorphism, Crystallinity and Hydrophilic–Lipophilic Balance of Stearic Acid and Stearic Acid–Capric/Caprylic Triglyceride Matrices for Production of Stable Nanoparticles. *Colloids Surf. B Biointerfaces* **2011**, *86*, 125–130. [CrossRef] [PubMed]
58. Pires, F.Q.; Angelo, T.; Silva, J.K.R.; Sá-Barreto, L.C.L.; Lima, E.M.; Gelfuso, G.M.; Gratieri, T.; Cunha-Filho, M.S.S. Use of Mixture Design in Drug-Excipient Compatibility Determinations: Thymol Nanoparticles Case Study. *J. Pharm. Biomed. Anal.* **2017**, *137*, 196–203. [CrossRef] [PubMed]
59. de Meneses, A.C.; Marques, E.B.P.; Leimann, F.V.; Gonçalves, O.H.; Ineu, R.P.; de Araújo, P.H.H.; de Oliveira, D.; Sayer, C. Encapsulation of Clove Oil in Nanostructured Lipid Carriers from Natural Waxes: Preparation, Characterization and in Vitro Evaluation of the Cholinesterase Enzymes. *Colloids Surf. A Physicochem. Eng. Asp.* **2019**, *583*, 123879. [CrossRef]
60. Ibrahim, S.S.; Salem, N.Y.; Abd ElNaby, S.S.; Adel, M.M. Characterization of Nanoparticles Loaded with Garlic Essential Oil and Their Insecticidal Activity Against Phthorimaea Operculella (Zeller) (PTM) (Lepidoptera: Gelechiidae). *Int. J. Nanosci. Nanotechnol.* **2021**, *17*, 147–160.
61. Adel, M.M.; Salem, N.Y.; Abdel-Aziz, N.F.; Ibrahim, S.S. Application of New Nano Pesticide Geranium Oil Loaded-Solid Lipid Nanoparticles for Control the Black Cutworm Agrotis Ipsilon (Hub.) (Lepi., Noctuidae). *Eur. Asian J. BioSci. Eurasia J. Biosci.* **2019**, *13*, 1453–1461.
62. Zayed, M. Silica Nanoparticles Boosted Abamectin's Acaricidal Bioactivity Against Tetranychus Urticae Koch's Two Spotted Spider Mite Developmental Stages. *J. Plant Prot. Pathol.* **2022**, *13*, 93–100. [CrossRef]
63. Sioutas, G.; Tsouknidas, A.; Gelasakis, A.I.; Vlachou, A.; Kaldeli, A.K.; Kouki, M.; Symeonidou, I.; Papadopoulos, E. In Vitro Acaricidal Activity of Silver Nanoparticles (AgNPs) against the Poultry Red Mite (*Dermanyssus gallinae*). *Pharmaceutics* **2023**, *15*, 659. [CrossRef]
64. Tortorici, S.; Cimino, C.; Ricupero, M.; Musumeci, T.; Biondi, A.; Siscaro, G.; Carbone, C.; Zappalà, L. Nanostructured Lipid Carriers of Essential Oils as Potential Tools for the Sustainable Control of Insect Pests. *Ind. Crops Prod.* **2022**, *181*, 114766. [CrossRef]
65. Kraiss, H.; Cullen, E.M. Efficacy and Nontarget Effects of Reduced-Risk Insecticides on Aphis Glycines (Hemiptera: Aphididae) and Its Biological Control Agent Harmonia Axyridis (Coleoptera: Coccinellidae). *J. Econ. Entomol.* **2008**, *101*, 391–398. [CrossRef]